HAL open science

Novel trehalose-based excipients for stabilizing nebulized anti-SARS-CoV-2 antibody

François Noverraz, Baptiste Robin, Solène Passemard, Bénédicte Fauvel, Jessy Presumey, Emilie Rigal, Alan Cookson, J. Chopineau, Pierre Martineau, Martin Villalba, et al.

To cite this version:

François Noverraz, Baptiste Robin, Solène Passemard, Bénédicte Fauvel, Jessy Presumey, et al.. Novel trehalose-based excipients for stabilizing nebulized anti-SARS-CoV-2 antibody. International Journal of Pharmaceutics, 2023, 630, pp.122463. 10.1016/j.ijpharm.2022.122463 . hal-03935985

HAL Id: hal-03935985

https://hal.umontpellier.fr/hal-03935985v1

Submitted on 23 Mar 2023

HAL is a multi-disciplinary open access archive for the deposit and dissemination of scientific research documents, whether they are published or not. The documents may come from teaching and research institutions in France or abroad, or from public or private research centers.

L'archive ouverte pluridisciplinaire **HAL**, est destinée au dépôt et à la diffusion de documents scientifiques de niveau recherche, publiés ou non, émanant des établissements d'enseignement et de recherche français ou étrangers, des laboratoires publics ou privés.

Distributed under a Creative Commons Attribution 4.0 International License

International Journal of Pharmaceutics 630 (2023) 122463

Contents lists available at ScienceDirect

International Journal of Pharmaceutics

journal homepage: www.elsevier.com/locate/ijpharm

Novel trehalose-based excipients for stabilizing nebulized anti-SARS-CoV-2 antibody

François Noverraz [a,1], Baptiste Robin [c,1], Solène Passemard [d], Bénédicte Fauvel [e], Jessy Presumey [e], Emilie Rigal [e], Alan Cookson [f], Joël Chopineau [b], Pierre Martineau [g], Martin Villalba [h], Christian Jorgensen [h], Anne Aubert-Pouëssel [b], Marie Morille [b,*], Sandrine Gerber-Lemaire [a,*]

[a] Group for Functionalized Biomaterials, Institute of Chemical Sciences and Engineering Ecole Polytechnique Fédérale de Lausanne, EPFL SB ISIC SCI-SB-SG, Station 6, CH-1015 Lausanne, Switzerland
[b] ICGM, Univ Montpellier, CNRS, ENSCM, Montpellier, France
[c] MedXCell Science, Bâtiment Cyborg 1 (IRMB), Hôpital Saint-Eloi, 80 avenue Augustin Fliche, 34295 Montpellier, France
[d] Montpellier Life Science Bâtiment Cyborg 1 (IRMB), Hôpital Saint-Eloi, 80 avenue Augustin Fliche, 34295 Montpellier, France
[e] CYTEA BIO, Bâtiment Cyborg 1 (IRMB), Hôpital Saint-Eloi, 80 avenue Augustin Fliche, 34295 Montpellier, France
[f] MedXCell SA, Av. des Planches 20C, 1820 Montreux, Suisse
[g] IRCM, Univ Montpellier, INSERM, ICM, Montpellier, France
[h] IRMB, Univ Montpellier, INSERM, CNRS, CHU Montpellier, Montpellier, France

ARTICLE INFO

Keywords:
Protein delivery
Lung disease
Nebulization
Antibody formulation
Stabilizing excipients
Succinylated trehalose

ABSTRACT

COVID-19 is caused by the infection of the lungs by SARS-CoV-2. Monoclonal antibodies, such as sotrovimab, showed great efficiency in neutralizing the virus before its internalization by lung epithelial cells. However, parenteral routes are still the preferred route of administration, even for local infections, which requires injection of high doses of antibody to reach efficacious concentrations in the lungs. Lung administration of antibodies would be more relevant requiring lower doses, thus reducing the costs and the side effects. But aerosolization of therapeutic proteins is very challenging, as the different processes available are harsh and trigger protein aggregation and conformational changes. This decreases the efficiency of the treatment, and can increase its immunogenicity.

To address those issues, we developed a series of new excipients composed of a trehalose core, a succinyl side chain and a hydrophobic carbon chain (from 8 to 16 carbons). Succinylation increased the solubility of the excipients, allowing their use at relevant concentrations for protein stabilization. In particular, the excipient with 16 carbons (C_{16}TreSuc) used at 5.6 mM was able to preserve colloidal stability and antigen-binding ability of sotrovimab during the nebulization process. It could also be used as a cryoprotectant, allowing storage of sotrovimab in a lyophilized form during weeks. Finally, we demonstrated that C_{16}TreSuc could be used as an excipient to stabilize antibodies for the treatment against COVID-19, by *in vitro* and *in vivo* assays. The presence of C_{16}TreSuc during nebulization preserved the neutralization capacity of sotrovimab against SARS-CoV-2 *in vitro*; an increase of its efficacy was even observed, compared to the non-nebulized control. The *in vivo* study also showed the wide distribution of sotrovimab in mice lungs, after nebulization with 5.6 mM of excipient.

This work brings a solution to stabilize therapeutic proteins during storage and nebulization, making pulmonary immunotherapy possible in the treatment of COVID-19 and other lung diseases.

1. Introduction

Severe acute respiratory syndrome coronavirus 2 (SARS-CoV-2) causative virus infects epithelial cells in the respiratory tract, which makes it a worldwide major burden causing coronavirus disease-19 (COVID-19) with severe inflammatory conditions to the lungs

* Corresponding authors.
E-mail addresses: marie.morille@umontpellier.fr (M. Morille), sandrine.gerber@epfl.ch (S. Gerber-Lemaire).
[1] contributed equally.

https://doi.org/10.1016/j.ijpharm.2022.122463
Received 19 October 2022; Received in revised form 23 November 2022; Accepted 27 November 2022
Available online 30 November 2022
0378-5173/© 2022 The Author(s). Published by Elsevier B.V. This is an open access article under the CC BY license (http://creativecommons.org/licenses/by/4.0/).

(Carsana et al., 2020). The viral membrane Spike protein is responsible for cell entry by interacting with the angiotensin-converting enzyme ACE2 present on the pneumocyte membrane (Song et al., 2018). To fight against the infection, anti-SARS-CoV-2 treatments based on monoclonal antibodies (mAbs) have gained considerable interest, as proteins often show high efficacy, and few side effects, thanks to their strong specificity towards their target (Leader et al., 2008). Some of them are able to neutralize SARS-CoV-2 virus before their entry into pneumocytes. In particular, S309 - an antibody isolated from a patient infected with SARS-CoV-1 - showed promising results against SARS-CoV-2 in prophylactic and therapeutic settings in animal models (Corti et al., 2021; Pinto et al., 2020). This antibody was optimized to obtain sotrovimab, which was marketed and administered by parenteral route for the treatment of patients being at high risk of developing a severe form of COVID-19 (EMA, 2021).

As far as therapeutic proteins on the market are concerned, the preferred routes of administration are parenteral because it maximizes bioavailability, as well as rapidity of action (Respaud et al., 2015). However, in the context of a pulmonary infection such as COVID-19, the passage of mAbs from the blood to the lung is very limited, requiring injection of very high doses of antibodies to obtain an effective concentration in the lungs (Roifman et al., 1987). The delivery of antibody drugs directly to the site of action via the pulmonary route is therefore an attractive alternative (Respaud et al., 2015). Antibody formulations developed for parenteral administration may not easily be repurposed for inhalation delivery. Among key parameters that must specifically be addressed, the formulation must preserve the integrity of inhaled proteins when they undergo mechanical and/or thermal stresses during aerosolization (Respaud et al., 2014). These different stresses can indeed trigger aggregation, conformation changes, or even cleavage of the proteins, resulting in a loss of efficacy and an increase in immunogenicity (Cui et al., 2017).

The amphiphilic properties of proteins can trigger changes in conformation, after their adsorption to an interface (Lee et al., 2011). As the bulk liquid is nebulized, the surface is dramatically increased, hence enhancing the risk of protein unfolding and aggregation following their adsorption at the air–liquid interface. A commonly used method to prevent interfacial damage on proteins is the use of nonionic surfactants. Among them, polysorbates (PS 20 and PS 80), widely used for parenteral administration of antibodies, have been successfully included in formulations for inhalation delivery of mAbs and proteins (Hertel et al., 2015; Respaud et al., 2014). However, several limitations of these excipients have been reported. First, polysorbates impair long-term storage due to the presence of peroxide residuals causing protein oxidation and enhancing protein degradation (Ha et al., 2002). Finally, it contains poly(ethylene glycol) (PEG), which is now known to provoke side effects due to the polymer itself after administration (specific and/or non-specific immunological response) (Guerrini et al., 2022; Hamad et al., 2008; Stone et al., 2019; Szebeni et al., 2011; Turecek et al., 2016; Yang et al., 2016). Finally, even if a number of protein therapeutics have been stably nebulized as part of chronic treatment regimens, to date, there has been no report on stable nebulization of a fully human mAb that has been advanced through late-stage clinical trials (Fröhlich and Salar-Behzadi, 2021). The challenges rely not only on the selection of appropriated excipients to be added in the formulation to stabilize mAb during nebulization, but also on the paucity of toxicity data on inhaled excipients and their potential impact on formulation properties, and thereby device performances (Liang et al., 2020; Mayor et al., 2021). Consequently, the nature and the concentration of these stabilisers should be kept to the minimum possible limit to reduce potential side effects (Montharu et al., 2010; Respaud et al., 2015).

In this framework, sugar-based surfactants are a good alternative to polysorbate surfactants. They display low toxicity, good biodegradability, good biocompatibility and are produced from cheaper and renewable sources (Naughton et al., 2019). While pharmaceutical, food, cosmetic, textile, oil, and agricultural applications manifest great interest in using biosurfactants for their benefits, their uses in pharmaceutical industries are limited due to the risk of endotoxin contamination when they are synthesized by microorganisms (Kügler et al., 2014; Kuyukina et al., 2015). Moreover, this mean of production results in glycolipids mixtures with different properties leading to inconsistent and unclear results (Ismail et al., 2021). Nevertheless, sugar-based surfactants have been recently synthetically produced circumventing those limitations. For instance, trehalose lipids that are constituted of trehalose attached through an ester bond to a lipid at various positions have been successfully synthesized (Bird et al., 2018; Jana et al., 2017; Jana and S. Kulkarni, 2020; Kale and Akamanchi, 2016; Schiefelbein, 2010). Thus, this work focused on the synthesis and formulation of surfactants based on natural and safe materials, trehalose, fatty acids, and succinate functionalities, for the stabilization of antibodies during nebulization. Trehalose is a two glucose units nonreducing disaccharide found in many plants, microorganisms, and animals. It is involved in many metabolism pathways and has been recognized to be very efficient for the protection and stabilization of cellular membranes and proteins through different mechanisms (Elbein et al., 2003; Jain and Roy, 2009; Lerbret et al., 2007; Lins et al., 2004; Moiset et al., 2014; Paul and Paul, 2015; Sudrik et al., 2017). This disaccharide is widely approved in biomolecules formulations for pharmaceutical development (Ohtake and Wang, 2011). Yet, to our knowledge, a trehalose fatty acid derivative with or without succinyl functionalities has never been used for the delivery of antibodies to the lung through nebulization.

During this study, trehalose-based excipients of different hydrophobic chain lengths were synthesized, and a succinyl moiety was added on the trehalose polar head. The ability of these excipients to preserve protein colloidal stability and binding ability was assessed after freeze-drying and/or nebulization. Biological *in vitro* efficacy and preliminary *in vivo* biodistribution studies were also performed. The proof of concept was carried out with sotrovimab, nebulized with a commercially available mesh nebulizer.

2. Material and methods

2.1. Material

D-(+)-Trehalose anhydrous, Succinic anhydride (TCI Europe), O-(Benzotriazol-1-yl)-N,N,N',N'-tetramethyluronium-tetrafluorborat (TBTU) (Carl Roth GmbH), Pyridine extra dry over molecular sieve (Thermo Scientific), Benzyl alcohol (Fluka), Myristic acid, Decanoic acid (Acros Organics), Octanoic acid, Palmitic acid (Fluorochem) were used as received without further purification.

For antibody formulation, sotrovimab antibody (PM = 146 kDa, pI = 8.42, monomer percentage = 97.1 %, sequence given in Supplementary Information S3) was synthesized by Evitria (Switzerland). Trehalose dihydrate and trehalose surfactants (C_8Tre, C_{10}Tre, C_{14}Tre and C_{16}Tre) were provided by Sigma-Aldrich (Merck, USA). Eumulgin SMO 20 (better known as polysorbate 80, or PS80) was purchased to BASF (Germany). PBS was provided by ThermoFisher Scientific (USA). Water was purified (resistivity of 18.2 MΩ.cm at 25 °C) using a MilliQ Direct Type 1 Ultrapure water system (Merck, USA).

For cytotoxicity, NIH-3 T3 cells were provided by American Type Culture Collection (ATCC) (USA). Cell viability assay (CellTiter 96® Aqueous Non-Radioactive Cell Proliferation Assay) was purchased from Promega (USA). For antigen binding assays, SARS-CoV-2 Spike expressing HEK293 cells, blasticidin and normocin were provided by InvivoGen (USA), while Cohesion Bioscience (UK) provided mouse anti-human IgG antibody labelled with Alexa Fluor 488. For *in vitro* neutralization assays, Vero E6 cells were provided by ECACC (UK), while SARS-CoV-2 viral strain n°2020A00935-34 (described by CPP Ile-de-France III) was from the CRB collection of Centre Hospitalier Universitaire de Montpellier (France). Control neutralizing antibodies (rabbit antibody, reference 40592-R001) were bought from Sino Biological (China), and Viral ToxGlo™ Assay was purchased from Promega

(USA). Common items such as RPMI and DMEM culture medium, FBS, penicillin, streptomycin and glutamine were purchased from Thermo-Fisher Scientific (USA).

For *in vivo* lung distribution studies, C57BL/6 wild type male mice were provided by Janvier labs (France). Isoflurane, ketamine and xilazine were purchased from Virbac (France), while PBS solution with PFA 4 % was purchased from Thermo Fisher Scientifics (USA), as well as Normal Fish Serum. Sucrose, Triton X-100 and Rabbit anti-human IgG were purchased from Sigma-Aldrich (USA). Secondary goat anti-rabbit coupled with Alexa Fluor 488 were purchased from Abcam (UK), Optimal Cutting Temperature compound NEG-50 MM was provided by MM Microm Microtech (France), Dako fluorescent mounting medium was provided by Agilent (USA), and ELISA kit for human IgG quantification was provided by BioRad (USA).

2.2. Characterization of trehalose derivatives

2.2.1. Nuclear magnetic resonance (NMR)

NMR spectra were recorded on Bruker Avance III-400 or Bruker Avance NEO spectrometers at room temperature (rt) (400 MHz) (Bruker, Billerica, MA, USA). ^{1}H frequency is at 400.13 MHz, ^{13}C frequency is at 100.62 MHz. Chemical shifts are expressed in parts per million (ppm) and coupling constants (J) in hertz (Hz). Solvent used for NMR spectroscopy was deuterated methanol (CD_3OD, Eurisotop).

2.2.2. Mass spectrometry

Mass spectrometry analyses were performed either on:

LTQ Orbitrap FTMS instrument (LTQ Orbitrap Elite FTMS, Thermo Scientific, Bremen, Germany) operated in the positive ionization mode coupled with a robotic chip-based nano-ESI source (TriVersa Nanomate, Advion Biosciences, Ithaca, NY, U.S.A.). A standard data acquisition and instrument control system was utilized (Thermo Scientific) whereas the ion source was controlled by Chipsoft 8.3.1 software (Advion BioScience). Samples were loaded onto a 96-well plate (Eppendorf, Hamburg, Germany) within an injection volume of 5 μL. The experimental conditions for the ionization voltage was + 1.4 kV and the gas pressure was set at 0.30 psi. The temperature of ion transfer capillary was 275 °C. FTMS spectra were obtained in the 100–1200 *m/z* range in the reduce profile mode with a resolution set to 120,000. In all spectra one microscan was acquired with a maximum injection time value of 1000 ms.

Xevo G2-S QTOF mass spectrometer coupled to the Acquity UPLC Class Binary Solvent manager and BTN sample manager (Waters, Corporation, Milford, MA). The sample manager system temperature was maintained at 10 °C and the injection volume was 5 μL. Mass spectrometer detection was operated in positive ionization using the Zspray™ dual-orthogonal multimode ESI/APCI/ESCi® source. The TOF mass spectra were acquired in the resolution mode over the range of *m/z* 50–1200 at an acquisition rate of 0.036 *sec*/spectra. The instrument was calibrated using a solution of sodium formate (0.01 mg/L in isopropanol/H2O 90:10). A mass accuracy better than 5 ppm was achieved using a Leucine Enkephalin solution as lock-mass (200 pg/mL in ACN/H_2O (50:50)) infused continuously using the LockSpray source. Source settings were as follows: cone, 25 V; capillary, 3 kV, source temperature, 150 °C; desolvation temperature, 500 °C, cone gas, 10 L/h, desolvation gas, 500 L/h. Data were processed using MassLynx™ 4.1 software.

Waters Acquity-I-UPLC Classsystem (Waters Corporation, Milford, MA, USA) coupled with a Waters Vion IMs-QTof Mass Spectrometer equipped with LockSpray (Leucine-enkephalin (200 pg/μL). Nitrogen was used as collision gas. The instrument was controlled by Waters UNIFI 1.9.4 (3.1.0, Waters Corporation, Milford, MA, USA). Injection volume was 5 μL in bypass mode with a flow rate was 0.1 mL/min. The instrument was operated in positive polarity, sensitivity mode (33,000 FWHM at 556.2766 *m/z*). Data was acquired in HDMSe mode with a scan time of 1 s. The recorded mass range was from 50 to 1200 *m/z* for both low and high energy spectra. The collision energy was ramped from 20 to 40 V. The cone voltage was set to 30 V, capillary voltage was set to 2 kV and source offset was set to 50 V. Source temperature was set to 120 ∘C and desolvation temperature set to 500 °C. Cone gas flow rate was set to 50 L/h and desolvation gas flow rate was set to 1000 L/h.

2.2.3. Fourier-transform infrared spectroscopy (FTIR)

IR spectra were recorded on a PerkinElmer Frontier FT/IR spectrometer outfitted with a QUEST ATR accessory as neat films compressed onto a Zinc Selenide window. The spectra are reported in cm^{-1}; *s*, strong; *m*, medium, *w*, weak.

2.2.4. Critical micelle concentration (CMC)

Surfactants solutions in distilled water were made via serial dilution in the concentration range between 1 μM and 100 mM. The solutions were analyzed by dynamic light scattering (DLS) on a Zetasizer Nano ZS (Malvern Panalytical, UK). Each dilution was scanned 3 times at 25 °C. The micellar formation was measured at ~ 10 nm. The recorded scattering intensity (Derived Count Rate expressed in kilo counts per second [kpcs]) was used to describe the quantity of micelles in solution. Critical micelle concentrations were determined by plotting the log of kpcs versus the log of surfactant concentration and fitting to two linear regressions at high and low concentration. The intersection of the two linear regressions correspond to the CMC.

2.2.5. In vitro cytoxicity

NIH-3T3 cell line was cultured at 37 °C in a 5 % CO_2 atmosphere, in DMEM growth medium, supplemented with 100 U/mL penicillin and 100 μg/mL streptomycin, and 10 % of fetal bovine serum. In vitro cytotoxicity of trehalose-based surfactants was then assessed, following a standardized protocol described in normative documents (International Organization of Standardization, 2009) and publications (Arechabala et al., 1999). In a 96-well plate, 5.10^3 cells were deposited in each well, and left for 1 day at 37 °C in a 5 % CO_2 atmosphere. Surfactant solutions ranging from 0.0112 to 11.2 mM were prepared by dilution of the stock solution into the cell culture medium. Those diluted solutions were then deposited to the wells, and after 48 h of incubation a CellTiter 96® Aqueous Non-Radioactive Cell Proliferation Assay (Promega, Wisconsin, USA) was used to evaluate the cell viability following manufacturer's instructions. The absorbance was then recorded at 490 nm using Multiskan™ GO Microplate Spectrophotometer (Thermo Scientific™, Waltham, Massachusetts, USA). Mean triplicate values of cell viability were plotted against the surfactant concentration, and the half-maximal effective concentration (EC_{50}) was determined by non-linear regression, using a "sigmoidal dose–response with variable hill slope" (the bottom was constraint to a constant value of 0 and the top to 100). This analysis was performed with the software GraphPad Prism 9.2.0 (GraphPad Software, USA).

2.3. Synthesis protocols

All reactions were performed under argon atmosphere (1 atm). Glassware was dried for 12 hr in an oven (T greater than 100 °C) or flamed dried under vacuum. Reactions were monitored by TLC (Merck silica gel 60F254 plates, Merck, Darmstadt, Germany). Detection was performed by $KMnO_4$ stain. Purifications were performed by flash chromatography on silica gel (SiliCycle SiliaFlash P60, 230–400 mesh) or C_{18}-reversed phase silica gel (Merck 60757, 230–400 mesh). Solvent used for flash column chromatography elution: Dichloromethane and Methanol (Thommen-Furler AG). In this section are described the characterizations of **C_{16}TreSuc** and its intermediates. Others derivatives characterizations (C_{xx}Tre, C_{xx}TreSucBn and C_{xx}TreSuc for xx = 8, 12, 14, 16) are reported in detail in Supplementary Information S5-S23.

2.4. General procedure for the preparation of C_{xx}Tre (xx = 8, 12, 14, 16)

In a flame-dried round-bottomed flask equipped with a magnetic stir bar, the corresponding fatty acid (1.1 eq.) and TBTU (1.1 eq.) were dissolved in anhydrous pyridine (2 mL / 0.1 g of Trehalose). Trehalose (1 eq.) was then poured into the reaction mixture, and stirring was continued at r.t. for 96 hr under argon atmosphere. Pyridine was then removed under vacuum, and the resulting residue was purified by flash column chromatography using a solvent gradient of 5–20 % methanol in EtOAc:DCM (1:1), yielding the intermediate **C_{xx}Tre** mono esters as white solids (yield 30–65 %).

Characterization data for Trehalose 6-hexadecanoate (**C_{16}Tre**):

^{1}H NMR (400 MHz, MeOD) δ 5.10 (dd, J = 8.7, 3.7 Hz, 2H, C**H** e, e'), 4.38 (dd, J = 11.9, 2.2 Hz, 1H, OOC-C**H$_2$**′), 4.21 (dd, J = 11.9, 5.1 Hz, 1H, OOC-C**H$_2$**′'), 4.03 (ddd, J = 10.2, 5.1, 2.1 Hz, 1H, C**H** a), 3.88 – 3.75 (m, 4H, C**H** c, c', a', a'–C**H$_2$**′), 3.69 (dd, J = 12.0, 5.6 Hz, 1H, a'–C**H$_2$**′'), 3.49 (dt, J = 9.8, 3.8 Hz, 2H, C**H** d, d'), 3.39 – 3.34 (m, 2H, C**H** b, b'), 2.36 (t, J = 7.4 Hz, 2H, [CH$_2$]–C**H$_2$**COO), 1.62 (m, 2H, [CH2]–C**H$_2$**-CH$_2$COO-), 1.31 (s, 24H, -[C**H$_2$**]-), 0.96 – 0.88 (m, 3H, C**H$_3$**). **HRMS (ESI/QTOF) *m/z*:** [M + Na]$^+$ Calcd for $C_{28}H_{52}NaO_{12}^+$ 603.3351; Found 603.3356.

2.5. General procedure for preparation of C_{xx}TreSucBn (xx = 8, 12, 14, 16)

In a flame-dried round-bottomed flask equipped with a magnetic stir bar, succinic acid monobenzyl ester (**SAMBE**, for synthesis procedure, see Supplementary Information S4) (1.1 eq.) and TBTU (1.1 eq.) were dissolved in anhydrous pyridine (2 mL / 0.1 g of **C_{xx}Tre**). The corresponding intermediate **C_{xx}Tre** (1 eq.) was poured into the reaction mixture, and stirring was continued at r.t. for 96 hr under argon atmosphere. Pyridine was then removed under vacuum, and the resulting residue was purified by flash column chromatography using a solvent gradient of 5–20 % methanol in EtOAc:DCM (1:1), yielding the intermediate **C_{xx}TreSucBn** as white solids (yield 30–40 %).

Characterization data for Trehalose 6-hexadecanoate 6′-benzylsuccinate (**C_{16}TreSucBn**):

^{1}H NMR (400 MHz, MeOD) δ 7.40 – 7.28 (m, 5H, ar.), 5.15 (d, J = 1.6 Hz, 2H, C**H$_2$**-ar.), 5.07 (dd, J = 8.8, 3.7 Hz, 2H, C**H** e, e'), 4.39 (ddd, J = 11.9, 6.6, 2.2 Hz, 2H, a-C**H$_2$**′, a'–C**H$_2$**′), 4.26 – 4.17 (m, 2H, a-C**H$_2$**′', a'–C**H$_2$**′'), 4.04 (tt, J = 5.5, 2.7 Hz, 2H, C**H** a, a'), 3.80 (td, J = 9.3, 1.7 Hz, 2H, C**H** c, c'), 3.50 (dt, J = 9.8, 3.4 Hz, 2H, C**H** d, d'), 3.40 – 3.36 (m, 2H, C**H** b, b'), 2.70 (d, J = 1.9 Hz, 4H, OOC-C**H$_2$**-C**H$_2$**-COO), 2.34 (t, J = 7.4 Hz, 2H, [CH$_2$]–C**H$_2$**COO), 1.66 –1.58 (m, 2H, [CH2]–C**H$_2$**-CH2COO), 1.30 (s, 24H, -[C**H$_2$**]-), 0.92 (t, J = 6.8 Hz, 3H, C**H$_3$**). **^{13}C NMR (101 MHz, MeOD)** δ 172.5, 128.12, 127.76, 93.60, 73.14, 72.38, 71.84, 70.54, 66.11,33.41, 31.67–28.96, 28.78, 24.63, 22.33, 13.03. **HRMS (ESI/QTOF) *m/z*:** [M + Na]$^+$ Calcd for $C_{39}H_{62}NaO_{15}^+$ 793.3981; Found 793.3979.

2.6. General procedure for the preparation of C_{xx}TreSuc (xx = 8, 12, 14, 16)

The intermediate **C_{xx}TreSucBn** (1 eq.) was dissolved in MeOH (1 mL / 0.1 g of intermediate) in a 3 necks flask and the solution was placed under argon atmosphere before adding 10 % Pd/C (0.1 eq.). Argon was removed from the reactor and the reaction mixture was back flushed with hydrogen (1 atm, 3 times). The reaction was vigorously stirred at r.t for 4 hr (monitored by TLC) under hydrogen atmosphere. After completion of the reaction, the solution was filtered through a Celite pad and the filter cake was washed with MeOH. The filtrate was concentrated under reduced pressure and the residue was purified by reversed phase flash chromatography (H$_2$O:MeOH 20:80 with 0.1 % TFA). The fractions corresponding to the product were collected, concentrated in vacuo and lyophilized to yield the desired ionic surfactants as white solids (yield 58 – 64 %).

Characterization data for Trehalose 6-hexadecanoate 6′-succinate (**C_{16}TreSuc**):

^{1}H NMR (400 MHz, MeOD) δ 5.06 (dd, J = 5.1, 3.8 Hz, 2H, C**H** e, e'), 4.38 (ddd, J = 16.3, 11.8, 2.1 Hz, 2H, a-C**H$_2$**′, a'–C**H$_2$**′), 4.21 (dt, J = 11.8, 4.8 Hz, 2H, a-C**H$_2$**′', a'–C**H$_2$**′'), 4.04 (ddd, J = 10.1, 4.3, 2.2 Hz, 2H, C**H** a, a'), 3.79 (td, J = 9.3, 2.6 Hz, 2H, C**H** c, c'), 3.50 (dt, J = 9.8, 3.8 Hz, 2H, C**H** d, d'), 3.39 – 3.34 (m, 2H, C**H** b, b'), 2.72 – 2.56 (m, 4H, 2 × OOC-C**H$_2$**), 2.35 (t, J = 7.4 Hz, 2H, [CH$_2$]–C**H$_2$**COO), 1.61 (q, J = 7.2 Hz, 2H, [CH2]–C**H$_2$**-CH$_2$COO-), 1.29 (s, 24H, -[C**H$_2$**]-), 0.90 (t, J = 6.8 Hz, 3H, C**H$_3$**). **^{13}C NMR (101 MHz, MeOD)** δ 174.16, 173.18, 93.98, 73.09, 72.98, 71.72, 71.61, 70.49, 70.19,70.07, 63.44, 63.01, 33.65, 31.67–29.03, 31.67–29.00, 28.81, 24.66, 22.33. **HRMS (ESI/QTOF) *m/z*:** [M + Na]$^+$ Calcd for $C_{32}H_{56}NaO_{15}^+$ 703.3511; Found 703.3497.

2.7. Preparation of antibody solution

The surfactant was weighed and dissolved in PBS, whose pH was adjusted to 5.8 by use of the suitable amount of HCl 0.67 M prior the dissolution. The solution of surfactant was then mixed with the solution of antibody 6.3 mg/mL, for a final concentration of antibody set at 1 mg/mL.

2.8. Nebulization and retrieving of antibody solution

A volume of 500 μL of antibody solution was placed in the atomizing cup of a vibrating mesh nebulizer NEB-001, provided by Briutcare (China), and a 15-mL tube was fixed at the exit of the nozzle. The nebulizer was started, and the nebulization rate was set at 0.4 mL/min ("medium rate"). After the whole volume was nebulized, the aerosol was left to coalesce and fall to the bottom of the tube during 2 min. Then the solution could be retrieved and antibody stability could be assessed.

2.9. Freeze-drying of antibody solution

A storage stability study was performed on freeze-dried antibody. Shortly, antibody solutions were frozen by dipping them in liquid nitrogen, and then placed in a freeze-drier (Heto Powerdry LL3000, Thermo Fisher Scientific, US) overnight. The tubes were then hermetically sealed and kept at 4 °C until further stability assays.

2.10. Stability assays

2.10.1. Aggregation monitoring

The solutions were analyzed by dynamic light scattering (DLS) on a Malvern Zetasizer Nano ZS (Malvern Panalytical, UK) operating at 25 °C with a 633-nm He-Ne laser and 173° scattering angle. A sample volume of 75 μL was transferred undiluted to a polymethyl methacrylate sub-microcuvette. ZetaSizer software was fed with the characteristics of particle material ("protein", refraction index = 1.45 and absorption = 0.01) and dispersant (water, viscosity = 0.8872 cP and refraction index = 1.330). The data processing setting was set as "General Purposes". Each sample was analyzed three times, to determine the total area under curve (AUC) of the peaks corresponding to antibody aggregates on the non-negative least-square distribution. All the peaks whose distribution mean was higher than the one of the monomer peak (around 10 nm) were considered to represent aggregates.

2.10.2. Binding efficiency by antigen recognition assays

The stability of the antibody was evaluated by studying its ability to bind antigen expressed at the surface of a stably transfected cell line. Shortly, SARS-CoV-2 spike (D614)-expressing Human Embryonic Kidney (HEK) cells were cultured in RPMI medium, with 10 % of fetal bovine serum, 100 U/mL penicillin, and 100 μg/mL streptomycin. Blasticidin (10 μg/mL) was added to select the transfected cells only. After distributing 250 000 cells per well in a 96-well plate, cells were

incubated with 50 μL of formulations at 500 ng/ml of antibody, for 15 min at 4 °C. Cells were washed in PBS, and Alexa Fluor 488-conjugated mouse monoclonal anti-human Fc IgG (Cohesion Bioscience) diluted at 1/500 in PBS was added. After 15 min of incubation in the dark, at 4 °C, cells were washed again and analyzed by flow cytometry using FACS CANTO II (BD Bioscience, USA). Each condition was done in triplicate. Data treatment was then performed using FlowJo software. Live cells were gated, and the percentage of fluorescent-labelled cells (*i.e.* cells interacting with the antibody of interest) was estimated among those latter. A negative control was performed without the antibody of interest and used to set the baseline at 0.

2.10.3. In vitro neutralization assay

Vero E6 cells were seeded in culture in DMEM medium, with 10 % of fetal bovine serum, 1 % penicillin, and 1 % streptomycin. In a 96-well plate, 30,000 cells were deposited in each well, and left for 1 day at 37 °C in a 5 % CO_2 atmosphere. Antibody solutions were prepared, and diluted in DMEM 0 % FBS at concentrations ranging from 6.8 ng/mL to 5 μg/mL. A SARS-CoV-2 viral suspension was also prepared at 100-fold its $TCID_{50}$ (*i.e.* 5.10^6 PFU/mL). It was then mixed to the antibody solutions, and incubated for 1 h at 37 °C. These mixtures were then added to the Vero cells, in the corresponding well, before incubating for 96 h at 37 °C. Each plate contains negative controls (cells infected with no antibody) and positive controls (cells not infected, cells in contact with virus and control neutralizing antibody from 5 μg/mL to 40 ng/mL). Cell viability was quantified using Viral ToxGlo™ Assay kit (Promega) according to the manufacturer's recommendations. The signal was read with an EnVision microplate reader (Perkin Elmer). For each condition, an average of the 3 replicates was calculated, and the data were processed with GraphPad Prism software (GraphPad Software, USA). The neutralizing titer NT_{50} was calculated using [Inhibitor] vs response model (variable slope, four parameters).

To confirm the trends observed with luminescence values, the cells were also observed in brightfield with Evos FL Microscope (ThermoFisher Scientific, USA). An image of each well was recorded for qualitative assessment of the cytopathic effect of the virus on the cells in the presence or absence of the antibody. Those results were shown in Supplementary Information S27 only, with only 1 image for each triplicate (as they were always similar).

2.11. Droplet size measurement

A volume of 3.6 mL of antibody solution was deposited in the nebulizing cup of a vibrating mesh nebulizer NEB-001 (Briutcare, China). The nebulizer was then mounted on a Spraytec laser diffraction system (Malvern Panalytical, UK): the distance between the laser and the detector was of 8 cm, while nebulizer outlet was placed at 2 cm from the laser. The nebulization flow rate was set at 0.4 mL/min, and the experiment was performed at room temperature and ambient relative humidity. Six measurements were performed on the same sample: four measurements with a duration of 1 min, and two measurements with a duration of 4 min, in order to analyze the totality of the solution. Note the last analysis was stopped before the end of the measurement, due to the lack of solution. Data were then analyzed using Spraytec software (Malvern Panalytical, UK). An average value of d_{10}, d_{50}, d_{90} was given for the six measurements.

2.12. In vivo lung distribution studies

Four C57BL/6 wild type mice were treated with a solution of sotrovimab at 1 mg/mL, formulated with 5.6 mM of C_8TreSuc in PBS and one untreated mouse as a control was used in this study. The laboratory procedures comply with French legislation, which implements the European Directives (Reference Number: D3417223, APAFIS#23920-2020020320279696v3). Mice from the treated group were anaesthetized individually using 5 % of isoflurane for 2 min. A nebulization mask was homemade by setting the finger of a latex glove at the tip of a vibrating mesh nebulizer NEB-001 (Briutcare, China), and piercing it gently. The 4 mice were then individually treated by placing the muzzle in the nebulization mask and aerosol was administered during 1 min at a flow rate of 0.4 mL/min. Blood and lung were collected from 2 mice at 30 min (n = 2) and from the 2 other mice at 24 h (n = 2) after treatment for IgG quantification in blood and qualitative biodistribution assessment by histopathology.

2.12.1. Blood sampling and ELISA human IgG analysis

At each time point, the animals were anaesthetized using ketamine/xilazine mixture (100 and 10 mg/kg respectively) administered by intraperitoneal injection at 10 mL/kg. In anesthetized animals, 1 mL of blood was sampled by cardiac puncture and collected in a tube containing heparine-Na as anticoagulant. Samples were centrifuged for 15 min at 1000 × g (or 3000 rpm) at 2–8 °C within 30 min of collection. 200 μL of supernatant (plasma) was stored at −20 °C for ELISA analysis. Human IgG quantification of undiluted samples (100 μL/well) was performed in duplicated by ELISA method.

2.12.2. Lung sampling and immunohistology analysis

After blood sampling, mice were sacrificed by cervical dislocation. Then, each animal was transcardially perfused using PBS solution with PFA 4 % during 2 min. After perfusion, the chest was opened and both lungs were sampled. Lungs were collected in a fresh tube and fixed overnight with PFA 4 % at 4 °C. Following fixation, samples were incubated 24–48 h in two successive baths of 6 % and 30 % sucrose, embedded in Optimal Cutting Temperature and stored at −80 °C. Coronal sections (10 μm of thickness) were cut using cryostat apparatus (LEICA CM3050). Proximal, central and distal lung sections (three segments) were cut. For immunolabeling, three cryosections were blocked with 5 % Normal Fish Serum (NFS) and 0.1 % triton X-100 in PBS, incubated overnight at 4 °C with rabbit anti-human IgG diluted 1/500 in NFS/Triton/PBS (5 % NFS and 0.05 % Triton in 100 mL PBS 1X pH 7.4), washed with PBS and then incubated 1 h at RT with green secondary goat anti-rabbit Alexa Fluor 488 diluted at 1/10,000 in NFS/Triton/PBS (5 % NFS and 0.05 % Triton in 100 mL PBS 1X pH 7.4). After several PBS washes, cryosections were mounted in Dako fluorescent mounting medium (S3023) with DAPI (1/10,000). Confocal laser scanning microscope (CLSM) (SP8-UV confocal microscope, Leica, Germany) was used to obtain images. The fluorescence intensity, corresponding to the IgG concentration was quantified for each lung section using ImageJ software.

3. Results and discussion

3.1. Preparation and analysis of the excipients

The ionic surfactants were synthesized by desymmetrization of D-(+)-Trehalose via mono esterification of its primary alcohols with a fatty acid (n = 6, 8, 12, 14) in the presence of TBTU as coupling agent (Fig. 1). The resulting $\mathbf{C_{xx}Tre}$ mono esters were obtained in 30 to 65 % yield (Table 1). Purification of these intermediates by flash chromatography, using a slow gradient of eluent (MeOH 5 to 20 % in EtOAc:DCM 1:1), allowed to efficiently remove the side products resulting from the esterification of secondary alcohols. The second esterification was carried out in the presence of succinic acid mono benzyl ester (**SAMBE**) and TBTU, leading to the functionalization of the second primary alcohol in 30 to 49 % yield. The benzyl group was removed by Pd catalyzed hydrogenolysis to afford the ionic surfactants $\mathbf{C_{xx}TreSuc}$, presenting a carboxylate moiety and aliphatic chains of various lengths. An alternative pathway involving temporary protection of the secondary alcohols as trimethylsilyl ethers, followed by sequential esterification of the remaining primary alcohols, was investigated. However, the higher number of synthetic steps led to drastically lower yields and this route was consequently discarded.

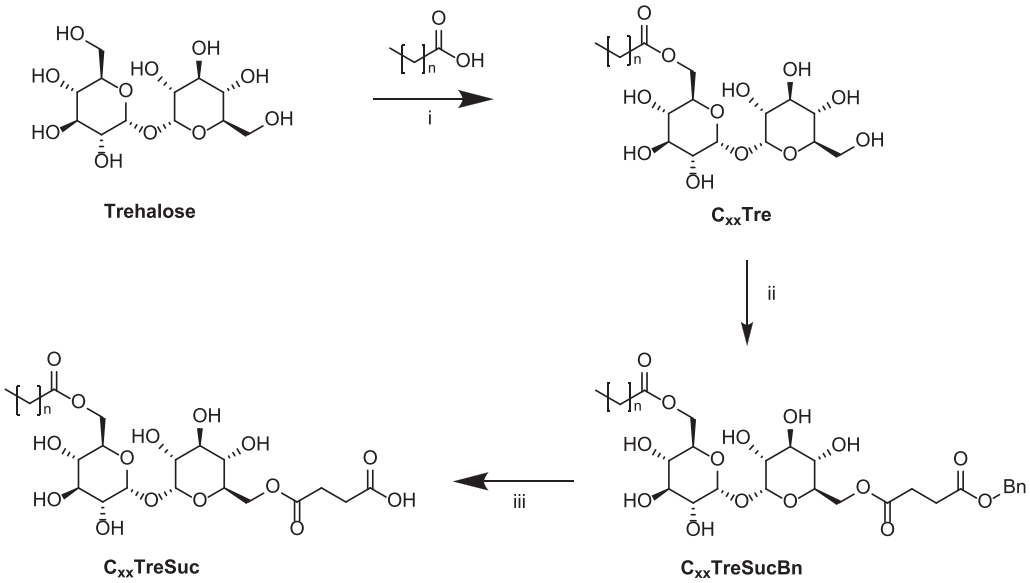

Fig. 1. Synthesis of Trehalose derived ionic surfactants. *Reagents and conditions: i- Fatty acid (n = 6, 8, 12, 14), TBTU, pyridine 96 hr. ii- SAMBE, TBTU pyridine 96 hr. iii- H_2 Pd/C, MeOH 3 hr.*

Table 1
Yields of intermediates and final surfactants with respect to the length of the fatty acid used (n = 6, 8, 12, 14).

Fatty acid	C_{xx}Tre	C_{xx}TreSucBn	C_{xx}TreSuc
Octanoate (n = 6)	40 %	49 %	60 %
Decanoate (n = 8)	30 %	40 %	63 %
Tetradecanoate (n = 12)	35 %	34 %	58 %
Hexadecanoate (n = 14)	65 %	30 %	64 %

As observed in Table 1, the yield varied between 39 and 65 % for the first step, 30 to 49 % for the second step and 58 to 64 % for the final step. These yields were reproducible throughout the numerous batches produced during this study. Also, there is no correlation between the yield of the reactions and the length of the fatty acid used but it is dependent on the type of reaction and purification strategy.

The critical micelle concentration (CMC) of the excipient can bring important insight on the behaviour of trehalose-based surfactants in aqueous medium, and provide valuable clues for the formulation. As a population of micelles must appear from CMC and at higher concentrations, CMC was assessed by DLS, measuring the derived count rate (correlated to the number of particles in suspension) as a function of the concentration for the different excipient solutions (graphical determinations are shown in the Supplementary Information, Figures S1, S2, S3). The results are shown in Table 2. First, it must be noticed that the derived count rate increase was mainly caused by the apparition of a peak at 5–10 nm (data not shown), which corresponds to spherical micelles of monoalkyl trehalose as described in the literature (Schiefelbein et al., 2010). However, **C_8TreSuc** did not seem to form this type of micelles, and the increase of scattering intensity was caused by larger structures (from few tens to few hundred nanometers). No further analysis of those structures was performed, but they might correspond to merged vesicles as suggested by another team working with non-succinylated **C_8Tre** (Kanemaru et al., 2012). Therefore, the DLS data were not exploitable for the CMC determination of **C_8TreSuc**. For the other surfactants, CMC results showed that the longer the alkyl chain, the lower the CMC, increasing from 0.07 mM for **C_{16}TreSuc** to 0.96 mM for **C_{10}TreSuc**. This is in good agreement with results obtained with other surfactants (Hanson et al., 2020). More interestingly, other groups have studied the CMC of non-succinylated trehalose monoalkyl derivatives (Chen et al., 2007). They showed the same increase of the CMC while reducing the length of the alkyl chain (30 mM for **C_8Tre**, 2.2 mM for **C_{10}Tre**, 0.21 mM for **C_{14}Tre** and 0.045 mM for **C_{16}Tre**). The influence of the succinylation could also be studied through CMC values. However, the direct comparison of CMC values between succinylated and non-succinylated trehalose surfactants is not relevant, as several publications showed that CMC values could be significantly different depending on the measurement method used (Hanson et al., 2020). For example, the CMC of non-succinylated **C_8Tre** was measured at 30 mM by the drop weight method (Chen et al., 2007), when another group who confronted tensiometry and pyrene fluorescence method obtained a CMC of 2.14 and 1.92 mM respectively (Schiefelbein et al., 2010).

Table 2
Critical Micellar Concentration of succinylated trehalose-based excipients, determined by DLS (n.d.: not determined).

Surfactant	C_{16}TreSuc	C_{14}TreSuc	C_{10}TreSuc	C_8TreSuc
CMC (mM)	0.07	0.67	0.96	n.d.

The cytotoxicity of all trehalose-based surfactants (succinylated or not) was assessed on NIH-3T3 cells after 48 h with a MTS cell viability test. **C_{16}Tre** could not be studied, due to its very low solubility (less than 5 mM for **C_{16}Tre** whereas **C_{16}TreSuc** was still soluble at a concentration of 800 mM in milli-Q water). EC_{50} were calculated by fitting dose–response models with experimental data, as shown in Supplementary Information S25) (Table 3). First, **C_8Tre** showed an EC_{50} value higher

Table 3
EC_{50} of the different excipients depending on the length of their carbon chain and the presence of a succinyl moiety, determined on NIH-3 T3 cells after 48 h of contact.

Carbon chain	C_8	C_{10}	C_{14}	C_{16}
Trehalose	greater than 11.2 mM	1.91 mM	0.21 mM	n.e.
Succinyl trehalose	3.61 mM	1.75 mM	0.34 mM	0.24 mM

n.e.: not evaluated.

than 11.2 mM, while **C_{10}Tre** and **C_{14}Tre** had EC_{50} of 1.91 mM and 0.21 mM respectively. This trend suggests that the longer the alkyl chain, the higher the cytotoxicity. This was confirmed by the EC_{50} of succinylated compounds, progressively decreasing from 3.61 mM (for **C_8TreSuc**) to 0.34 mM (for **C_{14}TreSuc**). Also, succinylation of the trehalose appeared to slightly increase the toxicity, as EC50 decreased from more than 11.2 mM to 3.61 mM after succinylation of **C_8Tre**. The same trend was observed for **C_{10}Tre**, although less pronounced (from 3.91 to 1.75 mM after succinylation). Indeed, succinyl group was probably negatively charged in the conditions of the experiment, as cells were maintained at pH = 7.4 (which is higher than the pK_a of most carboxylic acid). Yet, it is well known that anionic surfactants are more toxic than non-ionic surfactants, as they can generate electrostatic interactions with proteins (Lémery et al., 2015). However, if succinylation and long carbon chains seemed to increase cell toxicity, it was noticed that the chains of 14 or 16 carbons had very similar EC_{50} (0.21–0.34 mM), whether the trehalose was succinylated or not. In other words, there might be a toxicity threshold, above which increased number of carbons and succinylation have no more influence on the cytotoxicity of the compound. Interestingly, four of the trehalose-based surfactants studied were less toxic than PS80 (EC_{50} = 0.96 mM, which is close to other values found in the literature for similar experiments (Arechabala et al., 1999)), known itself for its low acute toxicity (Lansdown and Grasso, 1972). The three other surfactants were more toxic than PS80, but their respective EC_{50} remained in the same order of magnitude.

3.2. Trehalose-based excipients as antibody stabilizers during nebulization process

A first screening of the stabilizing conditions was made by monitoring the formation of antibody aggregates during nebulization of freshly prepared formulations. The nebulized mixture always contained 1 mg/mL of antibody, solubilized in PBS to have an isotonic medium, which avoids post-inhalation coughing reflex (Bonvini et al., 2016; Sahakijpijarn et al., 2020). The pH was adjusted to 5.8, thus remaining in the range of pH of commercial products (Wang and Ohtake, 2019; Warne, 2011). Depending on the samples, a trehalose-based excipient was also present, in various amounts. In the range of surfactants described in this study, we focused on the ones with the shortest and the longest carbon chain, respectively 8 and 16 carbons. This choice was made to show significant differences of behavior, depending on the chain length. However, as **C_{16}Tre** was not sufficiently soluble to be used, we worked mainly on the new succinylated trehalose-based surfactants, **C_8TreSuc** and **C_{16}TreSuc**.

The stability of the antibody during nebulization was assessed by DLS, following the area under the curve of aggregate peaks on the volume-weighed size distribution. As shown in Fig. 2, the presence of trehalose-based excipients can prevent the formation of aggregates, and their effect is proportional to their concentration. Indeed, when no excipient was used, antibody aggregates represented 0.6 % of the AUC in the fresh solution, while reaching 9.7 % after nebulization. When **C_8TreSuc** was added to the mixture (Fig. 2A), aggregation was dramatically restrained; aggregates increased from 2.1 to 4.6 % after nebulization with only 1 mM of **C_8TreSuc**. **C_{16}TreSuc** showed similar protective abilities, with aggregates proportion of 0.6 % before nebulization versus 4.9 % after nebulization with 1 mM of surfactant. If the excipient concentration was increased to 5.6 mM, a full protection of antibody against aggregation was achieved, whatever the carbon chain length (for **C_8TreSuc** and **C_{16}TreSuc**, shown in Fig. 2, but also for **C_{14}TreSuc** shown in Supplementary Information S26). The screening of the excipient concentration was performed once to select the best concentration of excipient in the formulation. Complete assessment of the formulations submitted to successive stress conditions (freeze-drying, storage and nebulization) can be found in triplicates in the next part of this study (see section 3.3).

Noticeably, the effective concentration was not related to the

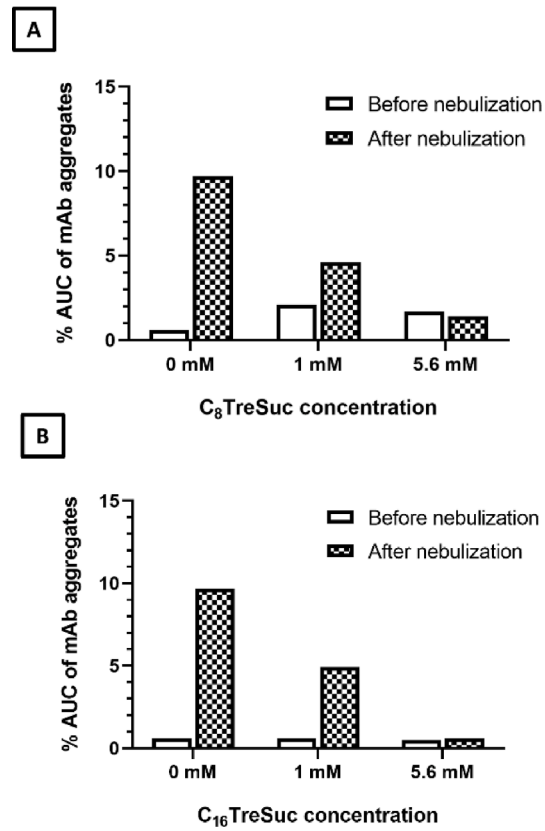

Fig. 2. Effect of nebulization on mAb aggregation in the presence of different concentrations of (A) **C_8TreSuc** or (B) **C_{16}TreSuc** (n = 1). Aggregation was monitored following the AUC of the aggregate peaks, relative to the total AUC of the volume-weighed size distribution obtained by DLS.

excipient CMC. Indeed, other excipients studied stabilized the antibody during nebulization when their concentration was set at 5.6 mM (see Supplementary Information S26), even if their CMC values were very different, ranging from 0.07 to 0.96 mM (Table 2). This absence of correlation between effective concentration and CMC is in good agreement with other results found in the literature (Cui et al., 2017; Mahler et al., 2009). This phenomenon arises from the fact that the optimal concentration for protein stabilization depends greatly on the interactions between the protein, the surfactant, and the interfaces. Indeed, the optimal concentration is reached when the surfactant molecules are numerous enough to cover all the interfaces and/or all the protein surface. This concentration can be considered as the CMC of the surfactant in solution containing proteins (Lee et al., 2011). It differs from the classical CMC, measured in pure water, hence the absence of correlation between the CMC measured in this work and the optimal stabilizing concentration for sotrovimab nebulization.

Then, the ability of the excipients to preserve the antibody functionality during nebulization was assessed *in vitro*. The antibody was solubilized with an effective concentration of excipient (5.6 mM of **C_8TreSuc** or **C_{16}TreSuc**), and nebulized. Nebulized and non-nebulized samples were then incubated with SARS-CoV-2 spike-expressing HEK293 cells. The proportion of antibodies that bind to cells was then assessed by FACS thanks to an AlexaFluor488-labelled secondary antibody. The binding of excipient-stabilized antibody, nebulized or not, was compared to the binding of non-stabilized antibody, in PBS only (Fig. 3). The results first show that 5.6 mM of trehalose-based excipient does not prevent the non-nebulized antibody from binding to Spike protein, as antibodies bound to 78 ± 1.6 % and 84 ± 1.2 % of cells when protected by **C_8TreSuc** or **C_{16}TreSuc** respectively, versus 80 ± 2.8 % of labelled-cells when no excipient was used. After nebulization, the

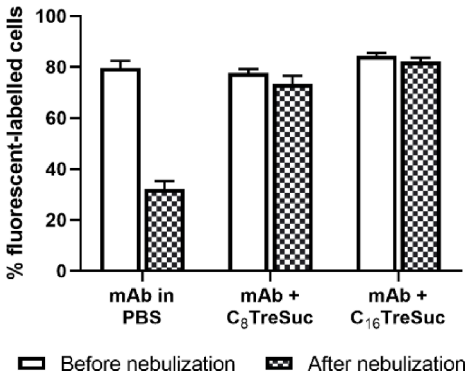

Fig. 3. Effect of nebulization on mAb binding to Spike-expressing HEK cells, depending on the presence or not of C_8TreSuc or C_{16}TreSuc at 5.6 mM. mAb binding was assessed by measuring the percentage of cells labelled by a fluorescent secondary antibody, by FACS and is expressed as the mean ± SD (3 independent experiments).

proportion of positive cells dramatically dropped to 32 ± 3.2 % when no excipient was used whereas in presence of trehalose-based excipient (5.6 mM) the proportion of positive cells remained unchanged (73 ± 3.2 % with **C_8TreSuc**, 82 ± 1.4 % with **C_{16}TreSuc**). Those results confirmed the stabilizing role of both **C_8TreSuc** and **C_{16}TreSuc** when used at 5.6 mM to protect antibodies against the different stresses occurring during nebulization.

3.3. Trehalose-based excipients as a cryoprotectant

While trehalose-based excipients were proven to be good stabilizers for nebulized antibodies in solution, we also investigated the interest of our synthesized excipients for long-term storage of the proteins in a dry form. Indeed, lyophilization is a common method to guarantee the stability of antibody formula stored for a long period of time. However, this process requires a freezing step and a drying step, that can trigger protein instability leading to a change of its conformation and thus its efficacy (Cui et al., 2017; Wang and Ohtake, 2019). Addition of sugar-based compounds (*e.g.* sucrose, trehalose) or surfactants (*e.g.* PS 80) have shown promise for preservation of protein structure during freeze-drying, the former acting as remarkable lyoprotectants and the latter as protein stabilizers during freezing (Wang, 2000). To demonstrate the cryopreservative property of our trehalose surfactants, antibody solutions with 5.6 mM of **C_8TreSuc** or **C_{16}TreSuc** were lyophilized and stored for 28 days at 4 °C, before assessing both the aggregation and the antigen-binding ability of the antibody. As shown in Fig. 4A, the formulation containing **C_8TreSuc** presented some aggregation (0.4 ± 0.1 % of aggregates on the volume weighed distribution before lyophilization, 3.6 ± 2.7 % after lyophilization and 28 days of storage) similar to the results obtained with formulation in PBS only (0.1 ± 0.1 % of aggregates before lyophilization, and 4.4 ± 2.7 % after lyophilization and 28 days of storage). Notably, the standard errors were high for those two conditions. Due to the non-quantitative value of DLS results, the proportion of detected aggregates was highly variable, when present in large amounts. This variability led us to consider the aggregation results with caution, despite the apparently high level of aggregation. Thus, antigen-binding assays were performed on the same samples, and the results were confirmed (Fig. 4B). A dramatic decrease of the cell binding was observed when antibody was solubilized in PBS alone (from 84 ± 0.6 to 9 ± 4 % after the process) or in the presence of 5.6 mM of **C_8TreSuc** (from 76 ± 0.6 % to 11 ± 9 %). On the contrary, **C_{16}TreSuc** prevented antibody from aggregating (Fig. 4A, 0.2 ± 0.1 % in the initial solution, and 0.1 ± 0.1 % after lyophilization and storage) and preserved its antigen-binding ability (Fig. 4B, 75 ± 1.6 % in the initial solution, versus 63 ± 7 % after lyophilization and storage). Thus, fatty acid chain length positively correlates with the antibody protection during lyophilization and storage. This can be explained by the stabilization mechanism itself. During lyophilization, protein conformation can change, and hydrophobic regions can be exposed to the outer surface, inducing destabilization of the proteins and increasing aggregation. The surfactant hydrophobic chain interacts with newly exposed hydrophobic regions of the protein, which prevents protein hydrophobic regions from interacting with each other, limiting irreversible conformation changes, and aggregation (Lee et al., 2006). Thus, **C_8TreSuc** might be less cryoprotective than **C_{16}TreSuc** because its shorter carbon chain confers lower hydrophobicity, hence decreased interaction with proteins during lyophilization.

Then, we challenged the cryoprotective performance of **C_{16}TreSuc** against other excipients commonly used in protein formulation. The cryoprotective performances of this innovative excipient were comparable to a formula containing 5 % of trehalose, commonly used for protein lyophilization (Kaushik and Bhat, 2003). However, trehalose alone had no protective effect during nebulization (data not shown), which made it less versatile than **C_{16}TreSuc**. More interestingly, **C_{16}TreSuc** was compared to PS80, recognized as a gold standard for protein stabilization, in liquid-form storage (Warne, 2011), but also during nebulization (Respaud et al., 2014; Sécher et al., 2022) or lyophilization (Ji et al., 2014). We studied the influence of **C_{16}TreSuc** and the reference PS80 surfactants on antibody aggregation and antigen-binding over the whole lifecycle of the drug. Thus, the antibody solution was prepared, lyophilized, stored for 28 days before being resuspended in purified water and nebulized. It appeared that PS80 did protect the antibody during its whole lifecycle. Antibody aggregates did not exceed 0.1 % of the total volume-weighed particle size distribution (Fig. 4A), and antigen-binding ability of antibody remained stable, between 68 ± 2 % before lyophilization, and 71 ± 4 % at the end of the lyophilization/storage/nebulization cycle (Fig. 4B). On the other hand, the novel excipient **C_{16}TreSuc** which previously showed great cryopreservation capacity also demonstrated its ability to preserve antibody colloidal stability (0.3 ± 0.2 % of aggregates) and binding ability (70 ± 2 %) after the whole lyophilization/storage/nebulization cycle. Thus, **C_{16}TreSuc** equals PS80 as a versatile excipient for antibody stabilization. But it also showed some advantages compared to polysorbates. Indeed, **C_{16}TreSuc** was conceived to be biodegradable, with hydrolysable ester bounds. After cleavage, the three released compounds are trehalose, succinic acid and palmitic acid, which are naturally present in the environment. It does not contain any PEG, unlike PS80, which is clearly an advantage regarding the issues recently highlighted by several groups about massive PEG use (Guerrini et al., 2022; Hamad et al., 2008; Stone et al., 2019; Szebeni et al., 2011; Turecek et al., 2016; Yang et al., 2016).

3.4. Therapeutic potential of the antibody after nebulization in the presence of trehalose-based excipients

3.4.1. In vitro neutralization assays

After demonstrating that trehalose-based excipients could help preserving antibody colloidal stability and antigen-binding ability, we aimed to show the interest of stabilizing Sotrovimab with these excipients for the treatment of COVID-19 by pulmonary way. To do so, we first demonstrated the potential of the formula to neutralize SARS-COV-2 virus *in vitro* after being nebulized. Wuhan variant virus was first mixed with nebulized antibody formulations, and then incubated with Vero E6 cells. The cytopathic effect caused by viral infection was measured and NT_{50} values were calculated (Table 4) (obtained from cell viability curves showed in Supplementary Information S25). The results indicated that, in the conditions of the experiment, at a concentration of 2.90 μg/mL, the non-nebulized antibody in PBS prevented half of the cells lysis. In the presence of 5.6 mM of nebulized **C_8TreSuc** formulation, the NT_{50} slightly decrease (NT_{50} = 2.02 μg/mL) and was divided by 3 with **C_{16}TreSuc** (NT_{50} = 0.95 μg/mL). The reliability of these surprising results was supported by the NT_{50} of the control neutralizing antibody, that was found to be 0.38 μg/mL in the conditions of this experiment,

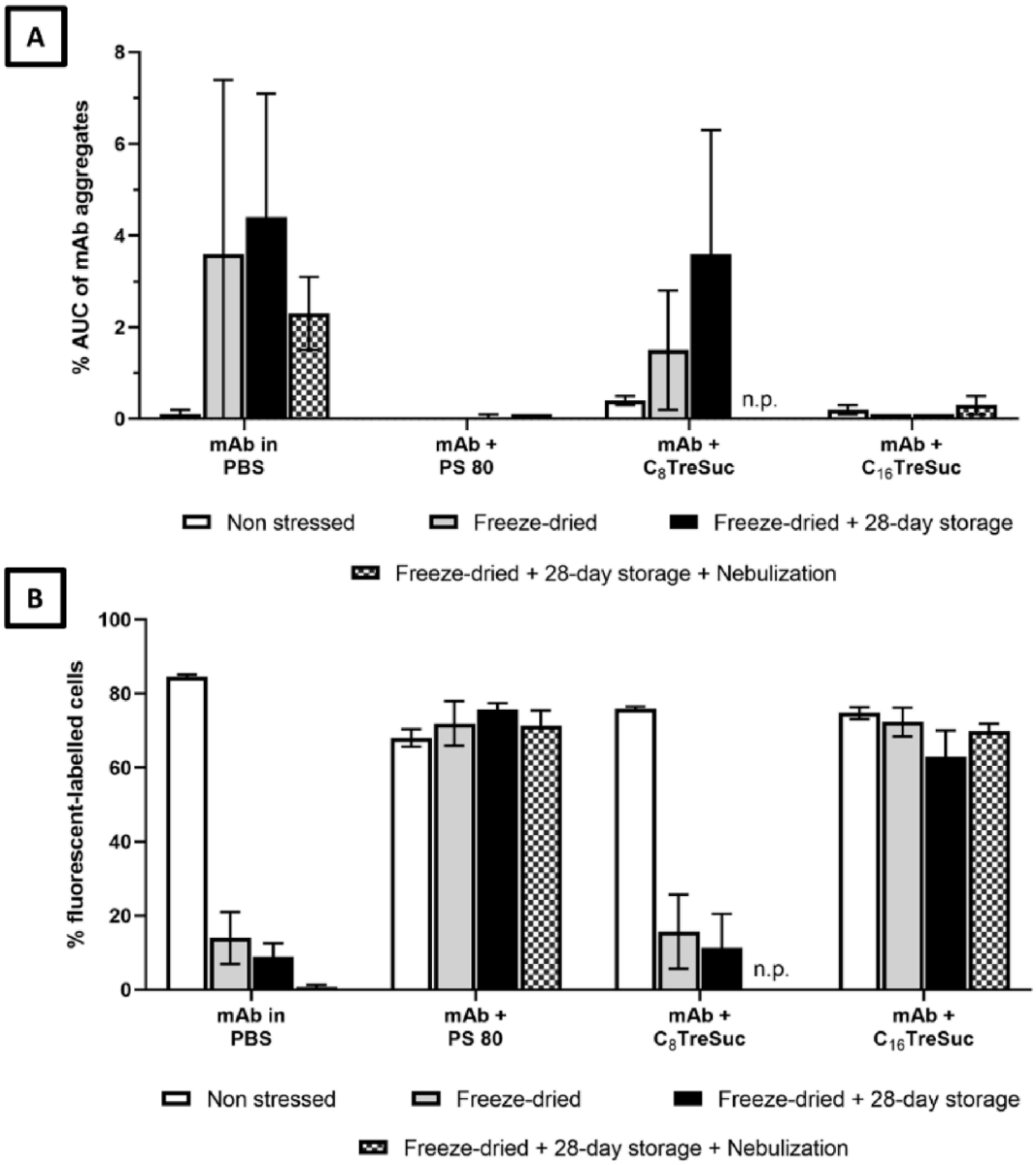

Fig. 4. Effect of freeze-drying, storage and nebulization (A) on mAb aggregation (monitored following the AUC of the aggregate peaks, relative to the total AUC of the volume-weighed size distribution obtained by DLS) and (B) on mAb binding to Spike-expressing HEK cells (assessed by measuring the percentage of cells labelled by a fluorescent secondary antibody, by FACS), depending on the presence or not of PS80, **C_8TreSuc** or **C_{16}TreSuc** at 5.6 mM. (n.p.: non performed). All values are expressed as the mean ± SD (3 independent experiments).

Table 4
NT_{50} of the antibody after nebulization in the presence of **C_8TreSuc** or **C_{16}TreSuc** 5.6 mM, measured in the conditions of the *in vitro* infection of Vero E6 cells by SARS-CoV-2. The control was a solution of antibody in PBS, with no excipient and no nebulization stress.

Sample	Non nebulized mAb in PBS	Nebulized mAb with C_8TreSuc	Nebulized mAb with C_{16}TreSuc
NT_{50} (µg/mL)	2.90	2.02	0.95

which is in the same order of magnitude as the provider's claims (0.29 µg/mL with WT SARS-CoV-2 Spike Pseudovirus). To explain the remarkable increase of neutralizing capacity of the antibody when nebulized in presence of **C_{16}TreSuc**, we first considered that the sotrovimab solution in PBS could have undergone instabilities during the incubation time with the virus (1 h at 37 °C). However, for all samples, no aggregation was detected by DLS after the incubation period (see Supplementary Information S28). A second hypothesis would be a favorable conformation change of sotrovimab, that could have been induced by the presence of **C_{16}TreSuc**, thus improving neutralization effect. Indeed, it was shown that PS80 and 20 can change the antibody conformation, without triggering aggregation (Singh et al., 2017). Further studies are needed to confirm this result.

3.4.2. *In vivo lung biodistribution studies*

Finally, a preliminary *in vivo* study was conducted to assess the antibody distribution in the lungs. C57BL/6 wild type mice were treated with a formula containing 1 mg/mL of antibody in PBS pH 5.8, stabilized with 5.6 mM of trehalose-based surfactant. Lung distribution was determined by labelling the human antibody of interest by immunohistochemistry in lung superior, middle and inferior lobes collected after 30 min or 24 h. As shown by CLSM images (Fig. 5A) and Mean Fluorescence Intensity measurements (MFI) (Fig. 5B), the nebulized

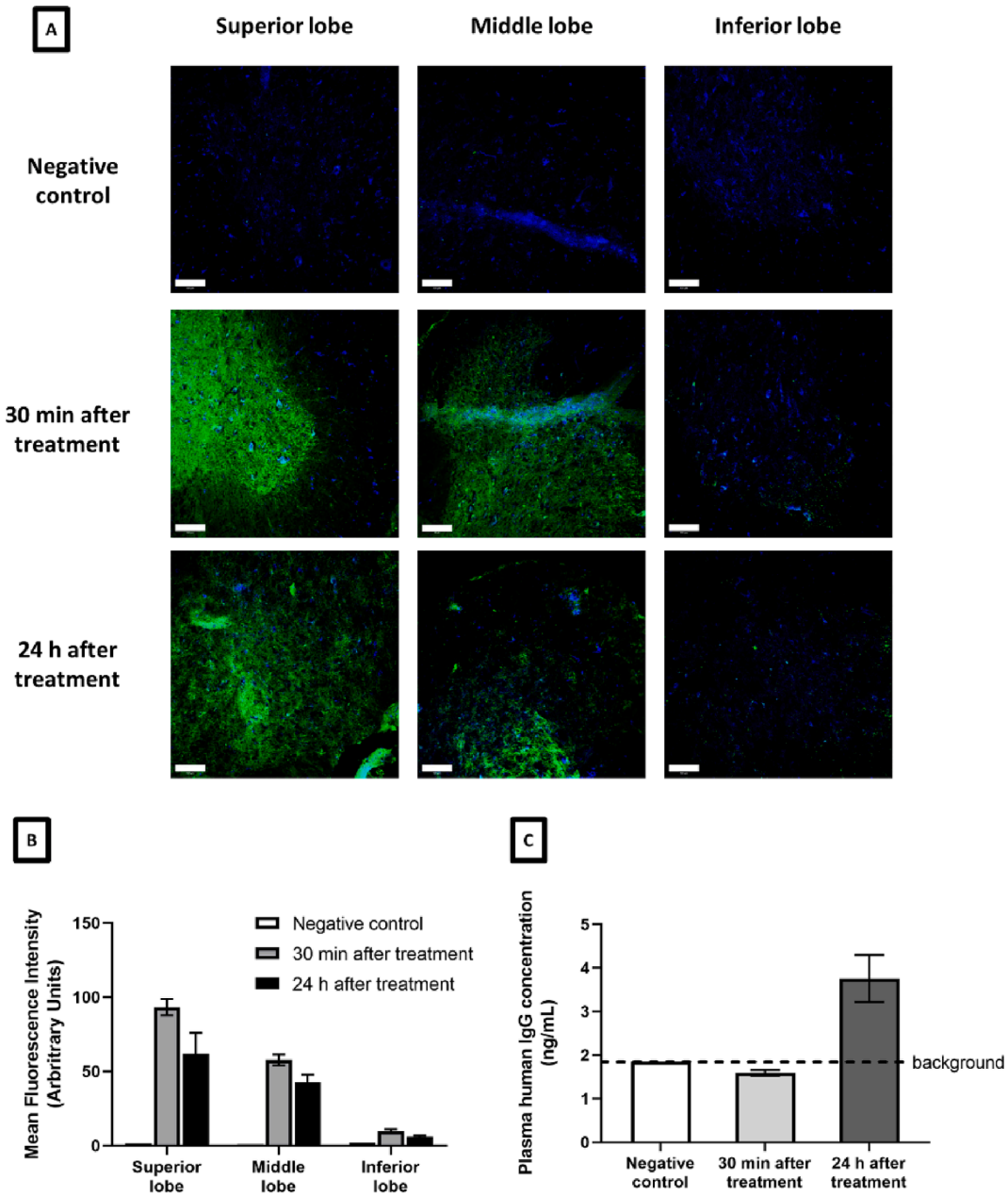

Fig. 5. Antibody biodistribution after treatment of C57BL/6 wild type mice, with 0.4 mL of a formula containing 1 mg/mL of antibody in PBS pH 5.8, stabilized with 5.6 mM of **C_8TreSuc**. (A, B) Lung distribution was determined by labelling human IgG of interest by immunohistochemistry on lung sections collected after 30 min or 24 h. Images shown in A are representative of what was observed on mice receiving the same treatment, and scale bar represents 100 μm. They were used to evaluate the mean fluorescence intensity of Alexa488, shown in B (1 value for the negative control, 2 independent values for the other conditions; mean ± SD). (C) Blood levels of human IgG determined by ELISA on blood samples, collected after 30 min or 24 h (1 value for the negative control, 2 independent values for the other conditions; mean ± SD).

antibody reached the superior and middle lobes and remained there in significant amounts after 30 min (93 AU in the superior lobe, 58 AU in the middle lobe). Comparatively, the inferior lobe contained very few antibodies, even though the MFI was higher than for the control mouse. This phenomenon was already observed for mice, and was explained by a preferential ventilation of the superior lobes in small rodents (Gu and Darquenne, 2021).

In superior and middle lobes, the antibody was homogenously distributed all over the cross section: this might mean the aerosolized formulation did not only deposit in the larger airways, but also in the alveoli (Bivas-Benita et al., 2005). This assumption was supported by the droplet size measurements, performed with Briutcare nebulizer by laser diffraction (Table 5). Nebulization of a solution of sotrovimab, at 1 mg/

Table 5
Droplet size distribution of aerosols containing the antibody 1 mg/mL in PBS pH 5.8, alone or stabilized with **C_{16}TreSuc** at 5.6 mM. Nebulization was performed with a vibrating mesh nebulizer NEB-001 (Briutcare) at a 0.4-mL/min flow rate. Six measurements were done on each sample, using a Spraytec laser diffraction system (Malvern Panalytical). Values are expressed as the mean ± SD (6 replicate measurements).

Sample	d_{10} (μm)	d_{50} (μm)	d_{90} (μm)
Sotrovimab in PBS	2.28 ± 0.02	4.82 ± 0.05	9.10 ± 0.12
Sotrovimab in PBS + C_{16}TreSuc 5.6 mM	2.41 ± 0.13	4.78 ± 0.04	8.92 ± 0.18

mL concentration, with or without the presence of excipient generated particles of median diameter d_{50} around 4.80 μm. This droplet size distribution was not influenced by the presence of trehalose-based excipient, the d_{10} and d_{90} being similar with or without **C_{16}TreSuc** at 5.6 mM (remaining respectively around 2.3 μm and 9.0 μm). According to recent reports, particles with a diameter below 5 μM deposit in the deep lungs, by diffusion, which means more than 50 % of the droplets would be able to reach the alveoli, while the rest would deposit in the bronchi and bronchioles (Carvalho et al., 2011). A more cautious threshold is sometimes proposed, considering that only particles smaller than 3 μm can deposit in the alveoli (Carvalho et al., 2011). This would still allow more than 10 % of the produced aerosol to reach the deeper lung (d_{10} = 2.41 μm), which supports the assumption that the aerosol was distributed in the whole airways. Considering that SARS-CoV-2 infection is characterized, in part, by alveoli injuries (Upadhya et al., 2022), such aerosol depth deposition might be useful in the perspective of a treatment for COVID-19 disease.

Beside the antibody distribution 30 min after the treatment administration, it is noteworthy that the antibody remained in the lung after 24 h, with MFI values of 62 AU in the superior lobe and 42 AU in the middle lobe (Fig. 5B). It is generally acknowledged that free antibody is eliminated from airways in less than 24 h by mucociliary clearance and by macrophages (Freches et al., 2017; Todoroff and Vanbever, 2011). However, other publications showed the presence of antibody several days after the nebulization treatment by immunochemistry assays (Guilleminault et al., 2014). We assumed that the antibody detected on CLSM images during immunohistochemistry assays was actually internalized by the lung epithelium.

Finally, the presence of the antibody in the plasma was quantified by ELISA, 30 min and 24 h after nebulization (Fig. 5C). The results showed a slow absorption of the antibody: antibody level was too low to be detected 30 min after nebulization, and it reached 3.8 ng/mL after 24 h. However, this level was still very low, compared to the concentration that would be obtained if the totality of the aerosolized antibody reached the lung and was absorbed through the alveoli walls (around 0.2 mg/mL for a mouse with 1.8 mL of blood). This suggests that a significant portion of the deposited antibody remained in the lung for at least 24 h, which is the targeted organ for COVID-19 treatment.

4. Conclusion

We developed new excipients that preserve antibody stability during nebulization process, allowing the administration of sotrovimab in lungs, for the treatment of COVID-19. Indeed, we synthesized a series of novel excipients composed of a succinylated trehalose polar head and a hydrophobic carbon chain of various length (from 8 to 16 carbons). Those excipients showed a higher solubility than their non-succinylated counterparts, allowing their use at relevant concentrations for protein stabilization. In particular, **C_{16}TreSuc** was proven to be an excellent candidate to preserve colloidal stability and antigen-binding ability of an antibody during the nebulization process. It also showed great advantages as a cryoprotectant, allowing to store antibodies in a lyophilized form for one month, at least. Finally, we demonstrated that **C_{16}TreSuc** could have potential uses in immunotherapy against COVID-19. The presence of **C_{16}TreSuc** during nebulization preserved the neutralization capacity of sotrovimab against SARS-CoV-2 *in vitro*; an increase of its efficacy was even observed, compared to the control. A preliminary *in vivo* study also showed the wide distribution of sotrovimab in mice lung, after nebulization with 5.6 mM of trehalose-based excipient. This study demonstrates the potential of trehalose-based excipients to stably nebulize human mAbs with no loss in binding and no aggregation. This opens the road for alternative excipients to replace usual stabilizers, such as polysorbates, for protein lung delivery.

Declaration of Competing Interest

The authors declare that they have no known competing financial interests or personal relationships that could have appeared to influence the work reported in this paper.

Data availability

The raw data associated to this study are available on Zenodo at: https://doi.org/10.5281/zenodo.7243350

Acknowledgements

The authors thank L. Menin and D. Ortiz (EPFL ISIC-MSEAP) for their support with MS characterizations and LC-MS quantifications, A. Bornet (EPFL ISIC-NMRP) for his assistance with NMR measurements. The present work has also benefited from the work of IDD-Xpert (France) for the droplet size analysis and InVivex (France) for the *in vivo* lung distribution study. We also acknowledge Centre d'Etudes des Maladies Infectieuses et Pharmacologie Anti-Infectieuse (UAR3725 CNRS – Université de Montpellier, France). MV and PM thank Labex MabImprove (ANR-10-LABX-53) for its support. This work was funded by research industrial grants at EPFL and ICGM.

Appendix A. Supplementary material

Supplementary data to this article can be found online at https://doi.org/10.1016/j.ijpharm.2022.122463.

References

Arechabala, B., Coiffard, C., Rivalland, P., Coiffard, L.J.M., Roeck-Holtzhauer, Y.D., 1999. Comparison of cytotoxicity of various surfactants tested on normal human fibroblast cultures using the neutral red test, MTT assay and LDH release. J. Appl. Toxicol. 19, 163–165. https://doi.org/10.1002/(SICI)1099-1263(199905/06)19:3<163::AID-JAT561>3.0.CO;2-H.

Bird, J.H., Khan, A.A., Nishimura, N., Yamasaki, S., Timmer, M.S.M., Stocker, B.L., 2018. Synthesis of branched trehalose glycolipids and their mincle agonist activity. J. Org. Chem. 83, 7593–7605. https://doi.org/10.1021/acs.joc.7b03269.

Bivas-Benita, M., Zwier, R., Junginger, H.E., Borchard, G., 2005. Non-invasive pulmonary aerosol delivery in mice by the endotracheal route. Eur. J. Pharm. Biopharm. 61, 214–218. https://doi.org/10.1016/j.ejpb.2005.04.009.

Bonvini, S.J., Birrell, M.A., Grace, M.S., Maher, S.A., Adcock, J.J., Wortley, M.A., Dubuis, E., Ching, Y.-M., Ford, A.P., Shala, F., Miralpeix, M., Tarrason, G., Smith, J. A., Belvisi, M.G., 2016. Transient receptor potential cation channel, subfamily V, member 4 and airway sensory afferent activation: Role of adenosine triphosphate. J. Allergy Clin. Immunol. 138, 249–261.e12. https://doi.org/10.1016/j.jaci.2015.10.044.

Carsana, L., Sonzogni, A., Nasr, A., Rossi, R.S., Pellegrinelli, A., Zerbi, P., Rech, R., Colombo, R., Antinori, S., Corbellino, M., Galli, M., Catena, E., Tosoni, A., Gianatti, A., Nebuloni, M., 2020. Pulmonary post-mortem findings in a series of COVID-19 cases from northern Italy: a two-centre descriptive study. Lancet Infect. Dis. 20, 1135–1140. https://doi.org/10.1016/S1473-3099(20)30434-5.

Carvalho, T.C., Peters, J.I., Williams, R.O., 2011. Influence of particle size on regional lung deposition – What evidence is there? Int. J. Pharm. 406, 1–10. https://doi.org/10.1016/j.ijpharm.2010.12.040.

Chen, J., Kimura, Y., Adachi, S., 2007. Surface activities of monoacyl trehaloses in aqueous solution. LWT Food Sci. Technol. 40, 412–417. https://doi.org/10.1016/j.lwt.2005.11.006.

Corti, D., Purcell, L.A., Snell, G., Veesler, D., 2021. Tackling COVID-19 with neutralizing monoclonal antibodies. Cell 184, 3086–3108. https://doi.org/10.1016/j.cell.2021.05.005.

Cui, Y., Cui, P., Chen, B., Li, S., Guan, H., 2017. Monoclonal antibodies: formulations of marketed products and recent advances in novel delivery system. Drug Dev. Ind. Pharm. 43, 519–530. https://doi.org/10.1080/03639045.2017.1278768.

Elbein, A.D., Pan, Y.T., Pastuszak, I., Carroll, D., 2003. New insights on trehalose: a multifunctional molecule. Glycobiology 13, 17R–27R. https://doi.org/10.1093/glycob/cwg047.

Ema, 2021. COVID-19: EMA recommends authorisation of antibody medicine Xevudy [WWW Document]. accessed 8.3.22 Eur. Med. Agency. https://www.ema.europa.eu/en/news/covid-19-ema-recommends-authorisation-antibody-medicine-xevudy.

Freches, D., Patil, H.P., Machado Franco, M., Uyttenhove, C., Heywood, S., Vanbever, R., 2017. PEGylation prolongs the pulmonary retention of an anti-IL-17A Fab' antibody fragment after pulmonary delivery in three different species. Int. J. Pharm. 521, 120–129. https://doi.org/10.1016/j.ijpharm.2017.02.021.

Fröhlich, E., Salar-Behzadi, S., 2021. Oral inhalation for delivery of proteins and peptides to the lungs. Eur. J. Pharm. Biopharm. 163, 198–211. https://doi.org/10.1016/j.ejpb.2021.04.003.

Gu, W., Darquenne, C., 2021. Heterogeneity in lobar and near-acini deposition of inhaled aerosol in the mouse lung. J. Aerosol Sci 151, 105642. https://doi.org/10.1016/j.jaerosci.2020.105642.

Guerrini, G., Gioria, S., Sauer, A.V., Lucchesi, S., Montagnani, F., Pastore, G., Ciabattini, A., Medaglini, D., Calzolai, L., 2022. Monitoring Anti-PEG Antibodies Level upon Repeated Lipid Nanoparticle-Based COVID-19 Vaccine Administration. Int. J. Mol. Sci. 23, 8838. https://doi.org/10.3390/ijms23168838.

L, Guilleminault, N, Azzopardi, C, Arnoult, J, Sobilo, V, Hervé, J, Montharu, A, Guillon, C, Andres, O, Herault, A, Le Pape, P, Diot, E, Lemarié, G, Paintaud, V, Gouilleux-Gruart, N, Heuzé-Vourc'h, Fate of inhaled monoclonal antibodies after the deposition of aerosolized particles in the respiratory system. Journal of Controlled Release 196 2014, 344 354. 10.1016/j.jconrel.2014.10.003.

Ha, E., Wang, W., Wang, Y.J., 2002. Peroxide formation in polysorbate 80 and protein stability. J. Pharm. Sci. 91, 2252–2264. https://doi.org/10.1002/jps.10216.

Hamad, I., Hunter, A.C., Szebeni, J., Moghimi, S.M., 2008. Poly(ethylene glycol)s generate complement activation products in human serum through increased alternative pathway turnover and a MASP-2-dependent process. Mol. Immunol. 46, 225–232. https://doi.org/10.1016/j.molimm.2008.08.276.

Hanson, M.G., Katz, J.S., Ma, H., Putterman, M., Yezer, B.A., Petermann, O., Reineke, T. M., 2020. Effects of hydrophobic tail length variation on surfactant-mediated protein stabilization. Mol. Pharmaceutics 17, 4302–4311. https://doi.org/10.1021/acs.molpharmaceut.0c00737.

Hertel, S.P., Winter, G., Friess, W., 2015. Protein stability in pulmonary drug delivery via nebulization. Adv. Drug Delivery Rev. Protein stability in drug delivery applications 93, 79–94. https://doi.org/10.1016/j.addr.2014.10.003.

International Organization of Standardization, 2009. ISO 10993-5:2009 : Biological evaluation of medical devices — Part 5: Tests for in vitro cytotoxicity.

Ismail, R., Baaity, Z., Csóka, I., 2021. Regulatory status quo and prospects for biosurfactants in pharmaceutical applications. Drug Discov. Today 26, 1929–1935. https://doi.org/10.1016/j.drudis.2021.03.029.

Jain, N.K., Roy, I., 2009. Effect of trehalose on protein structure. Protein Sci. 18, 24–36. https://doi.org/10.1002/pro.3.

Jana, S., Kulkarni, S.S., 2020. Synthesis of trehalose glycolipids. Org. Biomol. Chem. 18, 2013–2037. https://doi.org/10.1039/D0OB00041H.

Jana, S., Mondal, S., Kulkarni, S.S., 2017. Chemical Synthesis of Biosurfactant Succinoyl Trehalose Lipids. Org. Lett. 19, 1784–1787. https://doi.org/10.1021/acs.orglett.7b00550.

Ji, C., Sun, M., Yu, J., Wang, Y., Zheng, Y., Wang, H., Niu, R., 2014. Trehalose and Tween 80 Improve the Stability of Marine Lysozyme During Freeze-Drying. Biotechnol. Biotechnol. Equip.

Kale, S.S., Akamanchi, K.G., 2016. Trehalose monooleate: a potential antiaggregation agent for stabilization of proteins. Mol. Pharmaceutics 13, 4082–4093. https://doi.org/10.1021/acs.molpharmaceut.6b00686.

Kanemaru, M., Yamamoto, K., Kadokawa, J., 2012. Self-assembling properties of 6-O-alkyltrehaloses under aqueous conditions. Carbohydr. Res. 357, 32–40. https://doi.org/10.1016/j.carres.2012.05.014.

J.K, Kaushik, R, Bhat, Why Is Trehalose an Exceptional Protein Stabilizer: An analysis of the thermal stability of proteins in the presence of the compatible osmolyte trehalose. Journal of Biological Chemistry 278 2003 26458–26465. 10.1074/jbc.M300815200.

Kügler, J.H., Muhle-Goll, C., Kühl, B., Kraft, A., Heinzler, R., Kirschhöfer, F., Henkel, M., Wray, V., Luy, B., Brenner-Weiss, G., Lang, S., Syldatk, C., Hausmann, R., 2014. Trehalose lipid biosurfactants produced by the actinomycetes Tsukamurella spumae and T. pseudospumae. Appl. Microbiol. Biotechnol. 98, 8905–8915. https://doi.org/10.1007/s00253-014-5972-4.

Kuyukina, M.S., Ivshina, I.B., Baeva, T.A., Kochina, O.A., Gein, S.V., Chereshnev, V.A., 2015. Trehalolipid biosurfactants from nonpathogenic Rhodococcus actinobacteria with diverse immunomodulatory activities. New Biotechnol. Eur. Congress of Biotechnol. - ECB 16 (32), 559–568. https://doi.org/10.1016/j.nbt.2015.03.006.

Lansdown, A.B.G., Grasso, P., 1972. Physico-chemical factors influencing epidermal damage by surface active agents. Br. J. Dermatol. 86, 361–378. https://doi.org/10.1111/j.1365-2133.1972.tb05049.x.

Leader, B., Baca, Q.J., Golan, D.E., 2008. Protein therapeutics: a summary and pharmacological classification. Nat Rev Drug Discov 7, 21–39. https://doi.org/10.1038/nrd2399.

Lee, R.C., Despa, F., Guo, L., Betala, P., Kuo, A., Thiyagarajan, P., 2006. Surfactant copolymers prevent aggregation of heat denatured lysozyme. Ann. Biomed. Eng. 34, 1190–1200. https://doi.org/10.1007/s10439-006-9139-z.

Lee, H.J., McAuley, A., Schilke, K.F., McGuire, J., 2011. Molecular origins of surfactant-mediated stabilization of protein drugs. Adv. Drug Delivery Rev. Formulating biomolecules: mechanistics insights in molecular interactions 63, 1160–1171. https://doi.org/10.1016/j.addr.2011.06.015.

Lémery, E., Briançon, S., Chevalier, Y., Bordes, C., Oddos, T., Gohier, A., Bolzinger, M.-A., 2015. Skin toxicity of surfactants: structure/toxicity relationships. Colloids Surf A Physicochem. Eng. Asp. 469, 166–179. https://doi.org/10.1016/j.colsurfa.2015.01.019.

Lerbret, A., Bordat, P., Affouard, F., Hédoux, A., Guinet, Y., Descamps, M., 2007. How do trehalose, maltose, and sucrose influence some structural and dynamical properties of lysozyme? insight from molecular dynamics simulations. J. Phys. Chem. B 111, 9410–9420. https://doi.org/10.1021/jp071946z.

Liang, W., Pan, H.W., Vllasaliu, D., Lam, J.K.W., 2020. Pulmonary Delivery of Biological Drugs. Pharma. 12, 1025. https://doi.org/10.3390/pharmaceutics12111025.

Lins, R.D., Pereira, C.S., Hünenberger, P.H., 2004. Trehalose–protein interaction in aqueous solution. proteins: structure. Function, and Bioinformatics 55, 177–186. https://doi.org/10.1002/prot.10632.

Mahler, H.-C., Senner, F., Maeder, K., Mueller, R., 2009. Surface activity of a monoclonal antibody. J. Pharm. Sci. 98, 4525–4533. https://doi.org/10.1002/jps.21776.

A, Mayor, B, Thibert, S, Huille, R, Respaud, H, Audat, N, Heuzé-Vourc'h, Inhaled antibodies: formulations require specific development to overcome instability due to nebulization. Drug Deliv. and Transl. Res. 11 2021 1625–1633. 10.1007/s13346-021-00967-w.

Moiset, G., López, C.A., Bartelds, R., Syga, L., Rijpkema, E., Cukkemane, A., Baldus, M., Poolman, B., Marrink, S.J., 2014. Disaccharides impact the lateral organization of lipid membranes. J. Am. Chem. Soc. 136, 16167–16175. https://doi.org/10.1021/ja505476c.

Montharu, J., Le Guellec, S., Kittel, B., Rabemampianina, Y., Guillemain, J., Gauthier, F., Diot, P., de Monte, M., 2010. Evaluation of lung tolerance of ethanol, propylene glycol, and sorbitan monooleate as solvents in medical aerosols. J. Aerosol Med. Pulm. Drug Deliv. 23, 41–46. https://doi.org/10.1089/jamp.2008.0740.

Naughton, P.J., Marchant, R., Naughton, V., Banat, I.M., 2019. Microbial biosurfactants: current trends and applications in agricultural and biomedical industries. J. Appl. Microbiol. 127, 12–28. https://doi.org/10.1111/jam.14243.

Ohtake, S., Wang, Y.J., 2011. Trehalose: current use and future applications. J. Pharm. Sci. 100, 2020–2053. https://doi.org/10.1002/jps.22458.

Paul, S., Paul, S., 2015. Molecular Insights into the Role of Aqueous Trehalose Solution on Temperature-Induced Protein Denaturation. J. Phys. Chem. B 119, 1598–1610. https://doi.org/10.1021/jp510423n.

Pinto, D., Park, Y.-J., Beltramello, M., Walls, A.C., Tortorici, M.A., Bianchi, S., Jaconi, S., Culap, K., Zatta, F., De Marco, A., Peter, A., Guarino, B., Spreafico, R., Cameroni, E., Case, J.B., Chen, R.E., Havenar-Daughton, C., Snell, G., Telenti, A., Virgin, H.W., Lanzavecchia, A., Diamond, M.S., Fink, K., Veesler, D., Corti, D., 2020. Cross-neutralization of SARS-CoV-2 by a human monoclonal SARS-CoV antibody. Nature 583, 290–295. https://doi.org/10.1038/s41586-020-2349-y.

R, Respaud, D, Marchand, C, Parent, T, Pelat, P, Thullier, J.-F, Tournamille, M.-C, Viaud-Massuard, P, Diot, M, Si-Tahar, L, Vecellio, N, Heuzé-Vourc'h, Effect of formulation on the stability and aerosol performance of a nebulized antibody. mAbs 6 2014 1347–1355. 10.4161/mabs.29938.

R, Respaud, L, Vecellio, P, Diot, N, Heuzé-Vourc'h, Nebulization as a delivery method for mAbs in respiratory diseases. Expert Opinion on Drug Delivery 12 2015 1027–1039. 10.1517/17425247.2015.999039.

Roifman, ChaimM., Levison, H., Gelfand, ErwinW., 1987. High-dose versus low-dose intravenous immunoglobulin in hypogammaglobulinaemia and chronic lung disease. The Lancet, Originally published as Volume 1, Issue 8541 329, 1075–1077. 10.1016/S0140-6736(87)90494-6.

Sahakijpijarn, S., Smyth, H.D.C., Miller, D.P., Weers, J.G., 2020. Post-inhalation cough with therapeutic aerosols: Formulation considerations. Adv. Drug Deliv. Rev. 165–166, 127–141. https://doi.org/10.1016/j.addr.2020.05.003.

Schiefelbein, L., 2010. Synthesis, characterization and assessment of suitability of trehalose fatty acid esters as alternatives for polysorbates in protein formulation. Eur. J. Pharm. Biopharm. 9.

Schiefelbein, L., Keller, M., Weissmann, F., Luber, M., Bracher, F., Frieß, W., 2010. Synthesis, characterization and assessment of suitability of trehalose fatty acid esters as alternatives for polysorbates in protein formulation. Eur. J. Pharm. Biopharm. 76, 342–350. https://doi.org/10.1016/j.ejpb.2010.08.012.

T, Sécher, E, Bodier-Montagutelli, C, Parent, L, Bouvart, M, Cortes, M, Ferreira, R, MacLoughlin, G, Ilango, O, Schmid, R, Respaud, N, Heuzé-Vourc'h, Aggregates Associated with Instability of Antibodies during Aerosolization Induce Adverse Immunological Effects. Pharmaceutics 14 2022 671. 10.3390/pharmaceutics14030671.

Singh, S.M., Bandi, S., Jones, D.N.M., Mallela, K.M.G., 2017. Effect of Polysorbate 20 and Polysorbate 80 on the Higher-Order Structure of a Monoclonal Antibody and Its Fab and Fc Fragments Probed Using 2D nuclear magnetic resonance spectroscopy. J. Pharm. Sci. 106, 3486–3498. https://doi.org/10.1016/j.xphs.2017.08.011.

Song, W., Gui, M., Wang, X., Xiang, Y., 2018. Cryo-EM structure of the SARS coronavirus spike glycoprotein in complex with its host cell receptor ACE2. PLoS Pathog. 14, e1007236.

Stone, C.A., Liu, Y., Relling, M.V., Krantz, M.S., Pratt, A.L., Abreo, A., Hemler, J.A., Phillips, E.J., 2019. Immediate hypersensitivity to polyethylene glycols and polysorbates: more common than we have recognized. the journal of allergy and clinical immunology. In Pract. 7, 1533–1540.e8. https://doi.org/10.1016/j.jaip.2018.12.003.

Sudrik, C., Cloutier, T., Pham, P., Samra, H.S., Trout, B.L., 2017. Preferential interactions of trehalose, L-arginine.HCl and sodium chloride with therapeutically relevant IgG1 monoclonal antibodies. MAbs 9, 1155–1168. https://doi.org/10.1080/19420862.2017.1358328.

Szebeni, J., Muggia, F., Gabizon, A., Barenholz, Y., 2011. Activation of complement by therapeutic liposomes and other lipid excipient-based therapeutic products: prediction and prevention. Adv. Drug Delivery Rev., Complement Monotoring of Nanomed. Implants 63, 1020–1030. https://doi.org/10.1016/j.addr.2011.06.017.

Todoroff, J., Vanbever, R., 2011. Fate of nanomedicines in the lungs. Curr. Opin. Colloid Interface Sci. 16, 246–254. https://doi.org/10.1016/j.cocis.2011.03.001.

Turecek, P.L., Bossard, M.J., Schoetens, F., Ivens, I.A., 2016. PEGylation of Biopharmaceuticals: a review of chemistry and nonclinical safety information of approved drugs. J. Pharm. Sci. 105, 460–475. https://doi.org/10.1016/j.xphs.2015.11.015.

Upadhya, S., Rehman, J., Malik, A.B., Chen, S., 2022. Mechanisms of Lung Injury Induced by SARS-CoV-2 Infection. Physiology 37, 88–100. https://doi.org/10.1152/physiol.00033.2021.

Wang, W., 2000. Lyophilization and development of solid protein pharmaceuticals. Int J Pharm 203, 1–60. https://doi.org/10.1016/s0378-5173(00)00423-3.
Wang, W., Ohtake, S., 2019. Science and art of protein formulation development. Int. J. Pharm. 568, 118505 https://doi.org/10.1016/j.ijpharm.2019.118505.
Warne, N.W., 2011. Development of high concentration protein biopharmaceuticals: the use of platform approaches in formulation development. Eur. J. Pharma. Biopharmaceutics, Unmet Needs in Protein Formulation Sci. 78, 208–212. https://doi.org/10.1016/j.ejpb.2011.03.004.
Yang, Q., Jacobs, T.M., McCallen, J.D., Moore, D.T., Huckaby, J.T., Edelstein, J.N., Lai, S. K., 2016. Analysis of Pre-existing IgG and IgM Antibodies against Polyethylene Glycol (PEG) in the General Population. Anal. Chem. 88, 11804–11812. https://doi.org/10.1021/acs.analchem.6b03437.